Annals of Biomedical Engineering, Vol. 48, No. 2, February 2020 *(© 2019)* pp. 868–880
https://doi.org/10.1007/s10439-019-02426-7

Original Article

Straining 3D Hydrogels with Uniform *Z*-Axis Strains While Enabling Live Microscopy Imaging

AVISHY ROITBLAT RIBA, SARI NATAN, AVRAHAM KOLEL, HILA RUSHKIN, OREN TCHAICHEEYAN, and AYELET LESMAN

School of Mechanical Engineering, Faculty of Engineering, Tel-Aviv University, Tel-Aviv, Israel

(Received 11 August 2019; accepted 24 November 2019; published online 4 December 2019)

Associate Editor Smadar Cohen oversaw the review of this article.

Abstract—External forces play an important role in the development and regulation of many tissues. Such effects are often studied using specialized stretchers—standardized commercial and novel laboratory-designed. While designs for 2D stretchers are abundant, the range of available 3D stretcher designs is more limited, especially when live imaging is required. This work presents a novel method and a stretching device that allow straining of 3D hydrogels from their circumference, using a punctured elastic silicone strip as the sample carrier. The system was primarily constructed from 3D-printed parts and low-cost electronics, rendering it simple and cost-efficient to reproduce in other labs. To demonstrate the system functionality, > 100 μm thick soft fibrin gels (< 1 KPa) were stretched, while performing live confocal imaging. The subsequent strains and fiber alignment were analyzed and found to be relatively homogenous throughout the gel's thickness (Z axis). The uniform Z-response enabled by our approach was found to be in contrast to a previously reported approach that utilizes an underlying elastic substrate to convey strain to a 3D thick sample. This work advances the ability to study the role of external forces on biological processes under more physiological 3D conditions, and can contribute to the field of tissue engineering.

Keywords—Hydrogel, Extracellular matrix, Mechanobiology, Cell mechanics, Mechanical force, External stretching, Fibrous network, Fiber alignment.

INTRODUCTION

Response of cells to mechanical forces plays an important role in a wide range of biological functions, such as gene expression,[1,34] signaling,[39] and cell reorientation.[7,44] The response of the extracellular matrix (ECM) is also of great interest.[30,45] The fibrous mesh structure of the ECM have intriguing mechanical properties, such as nonlinear elasticity, non-affine deformation and reorientation under external strain.[41,50,51] A better understanding of how the ECM and its embedded cells respond to external mechanical forces will lead to more accurate computational and theoretical models and may advance the field of tissue engineering. One of the common ways to study these processes is to apply external force and strain the sample. Previous studies have mainly focused on stretching cells cultured on 2D planar substrates, demonstrating the direct effect of external stretch on cell behavior. For example, it was shown that in 2D, cells respond to external stretch by reorientating to various angles relative to the direction of applied stretch.[10,27,40,47] In comparison, the response of 3D constructs to external stretch, which more closely mimics the physiological context of many tissues, is much less understood.[19,25] It is currently clear that 3D samples behave differently under external strain than 2D samples, with different cellular orientations, protein expression levels and cell migrations in the z dimension.[2,32,36] Yet, the understanding of how different parameters, e.g., boundary conditions, loading profiles and matrix rigidity,[6,40] affect the response in 3D, remains very limited. This suggests that more efforts should be directed towards basic understanding of the response of 3D biological constructs to external strain, and towards better designs of stretchers uniquely built for 3D sample straining.

To date, many stretching devices for 3D constructs have been introduced by both commercial companies and research groups.[21] The stretching mechanisms and

Address correspondence to Ayelet Lesman, School of Mechanical Engineering, Faculty of Engineering, Tel-Aviv University, Tel-Aviv, Israel. Electronic mail: ayeletlesman@tauex.tau.ac.il

designs vary widely, including sleeve stretchers,[49] chamber stretchers,[28,52] clamping stretchers,[5,6] post stretchers,[4,18] cantilever stretchers,[14,46,53] and magnetic stretchers.[23,24] In these systems, a common benchmark for proof of concept is a predictable, preferably uniform, strain field in the X–Y plane. Usually, no data is given nor attention is invested in exploring the strain field in the z axis. In addition, the vast majority of stretchers do not allow for *in-situ* high-magnification imaging while stretching, and require sample fixation to visualize it under a confocal microscope. This is likely due to the challenging requirement of the confocal microscope, demanding the sample to be within a working distance of several hundred microns from the optical lens, particularly at high-magnifications. Systems that do allow for *in-situ* imaging of 3D constructs during gel stretching, manage this by adhering the sample directly to a thin planar elastic substrate, and imposing the external stretch to the underlying substrate.[8,16,30,33] However, by doing so, significant variations from uniform straining in the z axis may be introduced. The very few systems that do not compromise strain uniformity while imaging, do so by integrating non-linear optical microscopy (NLOM) techniques that do not limit the optical working distance, and are generally very complicated to reproduce in other labs. Examples of such systems include the 4-way clamping apparatus, which stretches the sample evenly from the sides, and an expanding sleeve apparatus, that mimics the expansion of blood vessels.[20,31]

In this work, we introduce the new Smart Cyclic Uniaxial Stretcher (SCyUS), which enables live confocal microscopy of static and cyclic uniaxial straining of thick, 3D soft gels. The device is based mainly on 3D printed parts and low-cost hardware. The system is designed to stretch elastic silicone strips with a puncture in their center. The 3D gel construct is polymerized into the dedicated puncture and adhered to its circumference, filling the hole with a gel-shaped disk that is strained when the strip is externally stretched. This combined system of the stretcher and gel-strip harbors a unique combination of features. Firstly, it allows for z-homogeneous straining of 3D soft gel constructs (e.g., fibrin, ~ 100 Pa) which are > 100 μm thick. These gels are too soft to be reliably made into free-standing strips or clampable scaffolds. It also supports inverted or upright live confocal microscopy. Further, the construction is low-cost, relying on 3D printing and an Arduino controller, so that it is easily reproducible in other labs. The strain regime and boundary conditions in the gel sample can be easily manipulated with the shape of the hole, enabling homogenous uniaxial or more advanced, tailored strain regimes. Lastly, it allows for use of miniature gel samples, with volumes as small as a few microliters.

To the best of our knowledge, no self-made system meeting all these conditions has been reported and successfully reconstructed in other labs. To encourage other labs to use and improve this technology, we provide a detailed description of the design challenges we have encountered, and share the full computer-aided design (CAD) and Python and Arduino codes for open-source use. Finally, to test the functionality of the stretching system, we applied increased static stretch of a soft fibrin gel and analyzed the gel strains and fiber reorientation in the z-gel depth axis using live confocal microscopy. In addition, we compared our stretching approach to a previously reported approach that uses an underlying elastic substrate to transfer external strain to 3D gels. We show that the use of substrate-based mechanism induces strong inhomogeneous strain in the z axis when a soft 3D gel thicker than a few tens of microns is used, exposing a yet seemingly unaccounted effect on analysis of 3D construct straining.

MATERIALS AND METHODS

Extended Method section is included in supplementary information (SI), Section 1.

Stretching Device Construction

The Smart Cyclic Uniaxial Stretcher (SCyUS) was designed using SolidWorks in order to be mostly 3D printed with a Fused Deposition Modeling (FDM) 3D printer, with only a few parts being made out of metal. For small parts, a FDM faculty printer (Ultimaker 3) was used using poly(lactic acid) (PLA). For larger parts, a commercial FDM printing service was used (Stratasys Fortus 450, ASA filament). Screw threading were metal inserts.

It is important to note that while the 3D-printed design requires some parts to have a manufacturing tolerance of ~ 50 μm due to optical considerations described later, these parts were made with a 3D printer that supports tolerances of ~ $\pm$ 200 μm, using methods elaborated on in the SI, Section 2. Establishing high 3D printing reliability maximizes flexibility for redesign and lab self-sufficiency.

The graphical user interface was written in Python using the Tkinter library, and the servo control was implemented by an Arduino Uno system that communicates with the said PC user interface.

Elaborate manufacturing instructions are described in the SI, as well as the full 3D CAD and code.

Silicone Strips

Silicone strips were made of 580 μm-thick silicone sheets (McMaster-Carr High Temperature Silicone Rubber), cut to 15 $\times$ 70 mm^2 strips. A dedicated hole in the middle of the strip was cut out using a hole puncher. The shape of the hole may vary, but the basic profile chosen for our experiments was a 1.5–2 mm diameter circular hole. A gel was polymerized into the hole, filling the entire thickness of the strip and naturally adhering to its circumference.

For the droplet-on-substrate experiments, the silicone strips were left unpunctured. The gel was polymerized as a droplet, directly on the silicone surface and gently flattened so the gel height did not exceed 300–400 μm for optical reasons. This droplet-type experiment represents the previously reported approach of using a stretchable substrate to transfer the strain to an adhered sample.[13]

To allow for convenient attachment of the silicone strip to the fabric length extenders using the printed clamps, we used a 3D printed mounting jig (SI Section 3).

Fiber Orientation Analysis

Gel fiber orientation was analyzed with OrientationJ (EPFL[11]) module of the ImageJ FIJI software (NIH[38]), using Gaussian gradient, and 1 pixel window. Nematic Order Parameter (NOP) of the orientation histogram was calculated as $\mathrm{N.O.P} = 2\left\langle (\cos\theta)^2 \right\rangle - 1$.[17] A score of N.O.P = 1 indicates perfect alignment along the axial direction (angle zero), N.O.P = 0 indicates isotropy and N.O.P = -1 indicates perfect alignment perpendicular to the axial direction (see example in Fig. 1).

Gel Polymerization in the Silicone Strip

3D gels were made by polymerizing the gels in the silicon punctuate. A hole in circular shape was cut out of a silicon strip, and the strip was then placed on a strip of parafilm in a 10 cm petri dish. 3 μL Fibrinogen solution (10 mg/mL, Omrix Biopharmaceuticals) was then placed in the hole, 3 μL thrombin solution (4 U/mL thrombin solution, Omrix Biopharmaceuticals) was added, and the mixture was then pipetted to mix the two solutions. Another parafilm strip was layered on top of the silicon strip, and then the area was flattened by gently pressing upon it with a flat object. The gel was then allowed to polymerize in the incubator at 37 °C for 20 min. After polymerization, the entire construct was submerged in PBS, and the parafilm layers were gently peeled off from the top and bottom sides. To ensure that the gel was adequate for sampling, the strip was loaded on the SCyUS and a z-stack tile imaging of the entire gel was taken to ensure homogeneity and adherence to the puncture circumference throughout the thickness of the silicone (SI, Section 4).

The fibrinogen was labeled with Alexa Fluor 546, succinimidyl ester (Invitrogen) by mixing the fibrinogen and Alexa Fluor at a molar ratio of 7.5:1, for 1 h, at room temperature and then filtering it through a HiTrap desalting column (GE Healthcare) packed with Sephadex G-25 resin to separate the unreacted dye.[15]

Cell Experiments

Actin-GFP 3T3 fibroblast cells (~ 8000 cells) were mixed with 3 μL Thrombin and added to the 3 μL fibrinogen solution, and then the mixture was placed in the silicone puncture for polymerization, in a similar

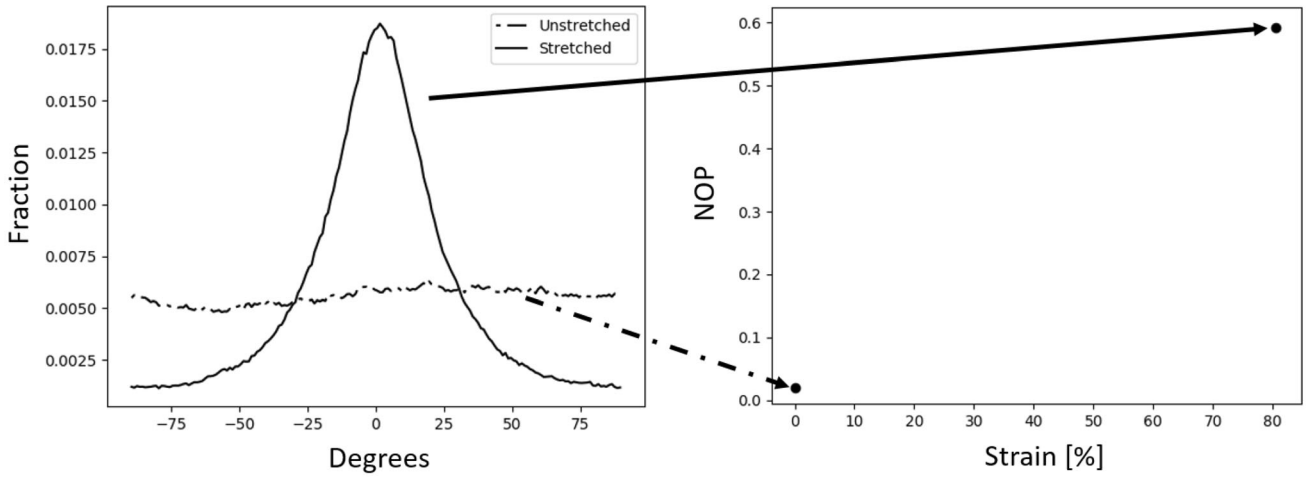

FIGURE 1. Analysis of fiber orientation using the OreintationJ tool (ImageJ software). Left—example of histograms calculated for stretched and unstretched gels. The histogram is normalized such that the area under the curve is 1. Right—the Nematic Order Parameter (NOP) calculated for each histogram, as a function of strain.

manner that was described in the section "Gel Polymerization in the Silicone Strip". The silicone-gel-cells construct was placed in the incubator for 3 h to allow initial attachment and spreading of cells in the gel, and then transferred to the SCyUS system for mechanical stretching and imaging with the confocal microscopy. The cellular gel construct was statically strained to 7% (hole axial strain) for up to 5 h. *Z*-stack confocal images were acquired after 3 and 5 h post-stretching.

RESULTS

Gel Straining Method

We developed a new method to strain 3D soft hydrogels that is based on stretching a silicone strip (elastic rubber) with a puncture (hole) in its center (Fig. 2). The hydrogel is polymerized into the dedicated puncture and adhere to its edge, filling the hole with a 3D gel that is strained from its perimeter when the strip is uniaxially stretched (Fig. 2). Specifically, we used fibrin gels, which were found to naturally and strongly adhere to the silicone. External stretching of the silicone strip results in straining of the fibrin gel, without any evidence of tearing or separation of the gel from the silicone (SI Section 5, Fig. S4). Details on the method of gel polymerization in the silicone puncture is described in the "Method" section. In this setup, strains occur along the direction of stretch (x-axis), as well as in the perpendicular directions (y- and z-axis), due to the Poisson effect (see schematic in Fig. 2b). Measurement of the Poisson ratio of the silicone hole (between its major axes) showed that it decreases during the stretching experiment (SI Section 6, Fig. S5).

Smart Cyclic Uniaxial Stretcher (SCyUS) Design and Construction

The SCyUS 3D-printed system was designed to apply static or cyclic uniaxial strain to soft 3D gels, while enabling live confocal inverted imaging. In order to induce gel strain, the silicone strip was clamped from both sides, one anchored statically (Fig. 3a, red part), while the other was connected to a spindle (Fig. 3a, blue part) that turns with a generic servo motor (Adafruit SG-5010).

While stretching, we aimed to use high-magnification imaging, and specifically targeted a × 40 water objective with a working distance of 600 μm ("Methods"). For that goal, designing a gap distance of 200 μm between the gel-strip and the glass coverslip (CS) would allow for an additional 400 μm of imaging into the depth of the gel. To ensure such a small gap distance, two height-affixing mechanisms were introduced—one for the aluminum liquid well containing the CS (Fig. 3a(iii), light grey part), and one for the silicone strip containing the gel. For the silicone strip, we used the pin-down insert (Fig. 3a, pink part), which forces a segment of about 20 mm of the strip between its two leading edges to a known height in a planner position. For the liquid well, a screw that controls the height of the well was integrated, enabling tunability of the height of the CS with respect to the gel, once the strip is in place (Fig. 3b, arrow 3). Moreover, the pin-down insert's side wings serve as a height limiter for the well, and prevents the CS from rising too close to the gel sample (Fig. 3a(iii), arrows). Thus, when the aluminum well sides touch the side wings of the pin-down insert, the distance between the gel sample and the coverslip is fixed (~ 200 μm).

In order to minimize X axis translation of the gel sample, the elastic part of the strip was kept at a minimal length, and extended with non-elastic fabric that made up the majority of the strip length (Fig. 2b in green, and Fig. 3b, arrow 2). The motor was controlled by an Arduino Uno connected to a Python Graphical User Interface (GUI) running on a PC. The current design is capable of stretching up to two silicone strips simultaneously, with the potential to include several gels within the same strip.

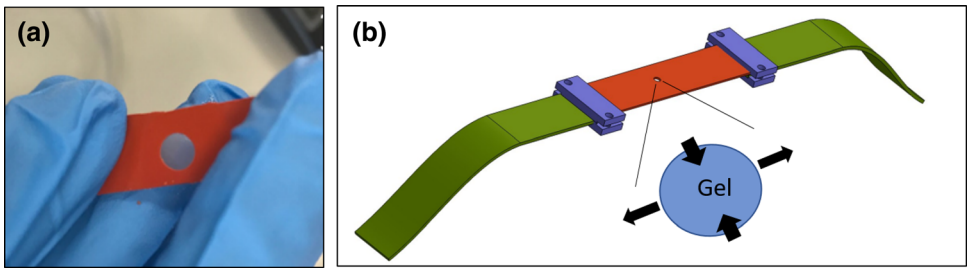

FIGURE 2. Hydrogel straining method. (a) A punctured silicone strip with an embedded fibrin gel. For illustration purposes, the hole in the silicone is much larger than in the actual experiments. (b) Illustration of the stretching approach with the silicone strip (orange), circular gel (hole in the middle), and extenders that connect the silicone to the stretching device (green). Enlarged area of the gel schematically show the deformation of the gel in response to uniaxial stretching of the silicone. For simplicity, the compression along the *z*-depth of the gel is not shown in the schematic.

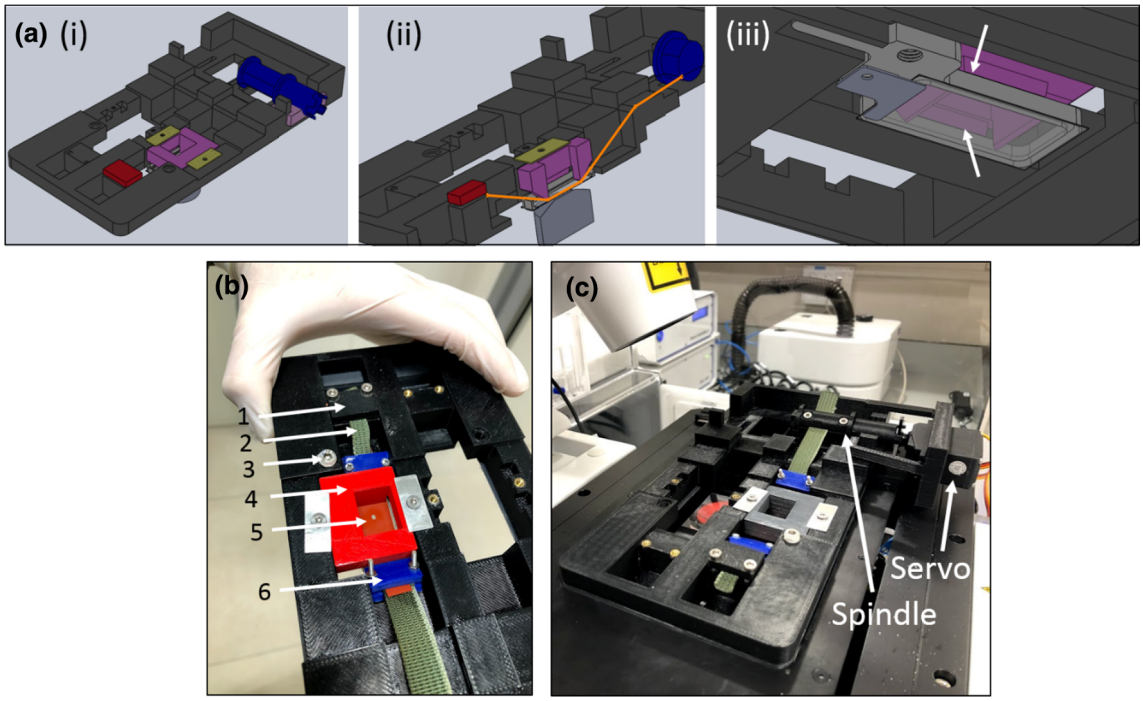

FIGURE 3. SCyUS stretching device. (a) Several views of a CAD model of the main parts of the SCyUS: spindle connected to the servo (blue), static anchor (red), insert that pins the silicone strip down (pink) and fixers that prevent the insert from rising up (yellow). A top view of the system (Ai), a cut view of the system (Aii) showing the path of the strip (orange line), and a bottom view (Aiii) of the aluminum liquid well with a translucent glass coverslip. The liquid well can be moved up and down with the turn of a screw fitted into the major threading. The upward movement of the aluminum well is limited by the pink insert's side wings, as shown by the white arrows. (b) The actual system with numbering indicating the (1) static anchor, (2) green non-stretchable fabric, (3) screw for aluminum liquid well height control, (4) red pin-down insert, (5) a brown punctuated silicone strip, (6) blue connecting clamps. (c) The stretching system placed on a confocal microscope. The servo motor and the spindle are shown with arrows.

SCyUS Operation

External stretch of the silicone strip induces average axial strain of the entire elastic strip of approximately 0.3% per degree of motor turn, and is referred to here as ε_{strip}. As the stretching is encoded by the Arduino software, every imaginable profile is applicable, bounded only by the resolution and the rotation speed of the motor implemented in the system. In our case, with the use of the Adafruit SG-5010 motor, the theoretical limits of SCyUS include cyclic strain of up to ~ 43% ε_{strip} in cycles as fast as 0.7 Hz. More details on ε_{strip} and cycle speed calculation are included in the SI, Section 7.

Also note, that the internal strains that develop in the gel enclosed in the punctured strip depend on the silicone strip length, gel shape (circular in our case) and size, and sampling location in the gel, and will be discussed later in more detail.

Gel Deformation

To understand how the gel deforms under the external stretch of the silicone, we first conducted finite element computer simulations of the stretched silicone-gel system (Fig. 4). The simulations indicate that the maximum principle strains develop in the direction of external stretch (x-axis), and are relatively uniform throughout the gel (Figs. 4a and 4b). Therefore, strain measurements in this circular configuration are not highly sensitive to the X–Y location in the gel. Due to the Poisson effect, both positive axial strains (ε_{xx}) and perpendicular negative strains (ε_{yy}) are developed (Fig. 4a). ε_{xx} and ε_{yy} are highly uniform along the x position (Fig. 4d), with minor changes along the y-position (Fig. 4c). The magnitude of the axial strains exceeds the perpendicular strains (Figs. 4c and 4d). Moreover, the relationship between the external strain of the silicone hole at its maximum radius (ε_{hole}) and the internal strains that develop in the center of the gel (ε_{gel}) was found to be linear with a slope of 1 (Fig. 4e). Finally, the Poisson ratio of the silicone hole was found to be within the range of the experimentally tested values (SI Section 6, Fig. S5).

We next experimentally evaluated the deformation of the gel in response to the silicone stretching. In the experiments, static stretch of increasing magnitudes was applied to the silicone strip loaded with fibrin gel embedded with 1 μm fluorescent beads. Low-resolu-

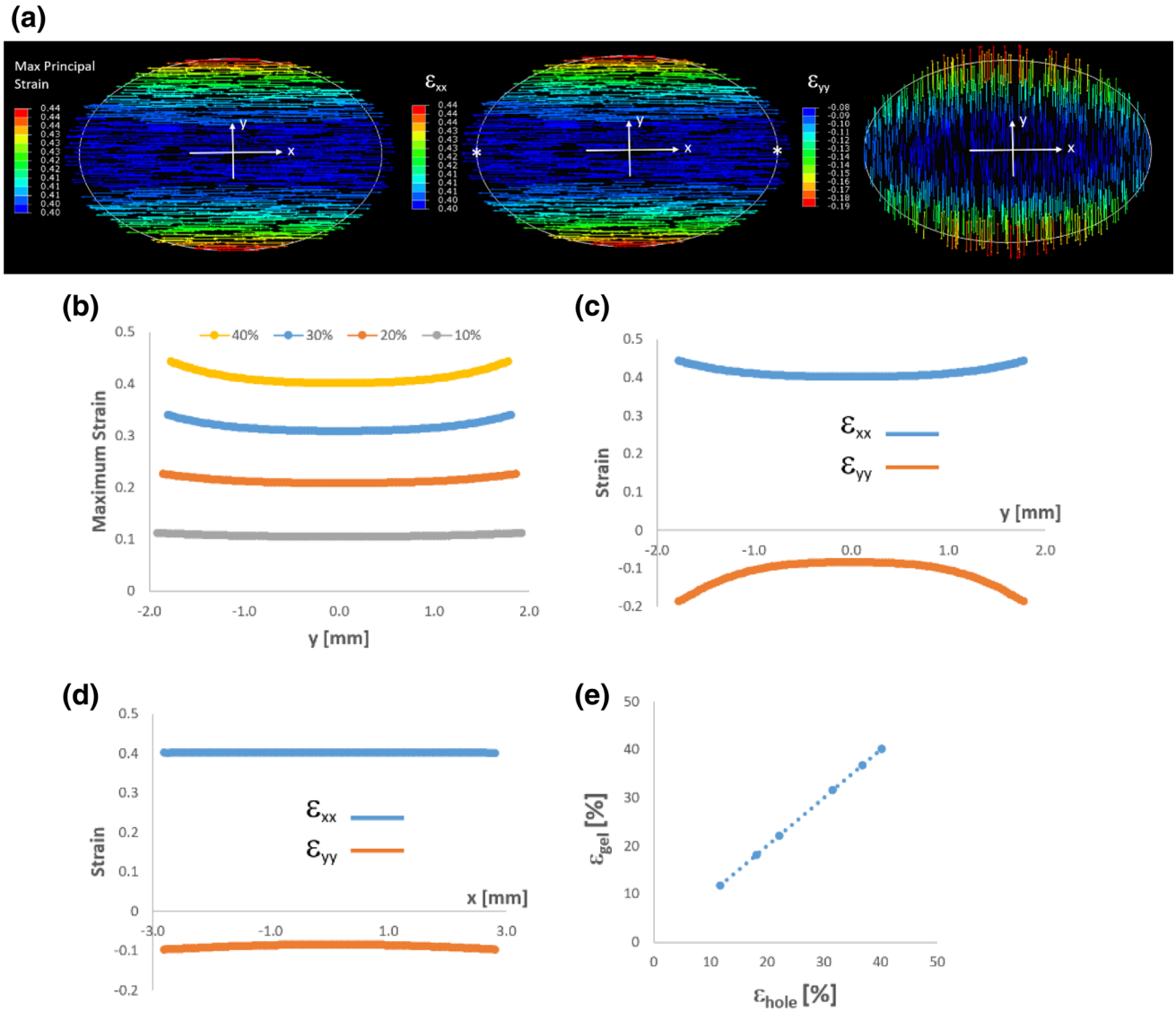

FIGURE 4. Computational simulations of a gel stretched in a circular silicone puncture. The silicone is not shown. (a) Color maps of maximum principal strains, axial strains (ε_{xx}), and perpendicular strains (ε_{yy}). The gel is stretched along the *x*-axis and compressed in the *y*-axis. (b) Quantification of maximum principal strains for several increasing stretch magnitudes of the silicone, measured at $x = 0$, as a function of *y* position. (c) Axial and perpendicular strains at $x = 0$, as a function of the *y* position. (d) Axial and perpendicular strains at $y = 0$, as a function of the *x* position. (e) Axial strains measured at the center of the gel (ε_{gel}) as a function of the axial strain of the hole (ε_{hole}), measured between to the two respective asterisks shown on the top central image in (a).

tion confocal *z*-stack tile imaging of the entire gel showed that as the silicone strip was stretched, the circular hole deformed and became more elliptical (Fig. 5a). Within a zoomed-in central area of the gel, several bead constellations were manually tracked as the gel was stretched. The results indicate that while the strip was axially strained by $\varepsilon_{strip} = 23\%$ (measured by the rotation of the spindle), the axial strain of the silicone hole at its maximum radius was $\varepsilon_{hole} = 64\%$, and the internal gel strain was $\varepsilon_{gel} = 46\%$ (at the center of the gel). All strains considered here are axial strains in the direction of the external stretch, see Fig. 4c for clarification. The graph in Fig. 5d indicates that the axial strain propagates relatively linearly from the silicone hole edge to the center of the gel, with a slope of approximately 0.74, which is a smaller slope than predicted by the simulations (Fig. 4e). Compression in the Y direction of the gel is also approximately linear as a function of X strain (Fig. 5d).

Gel Fiber Orientation

To characterize the structural response of the fibrous gel to increasing magnitudes of external stretch of the silicone, fiber alignment was measured by high-

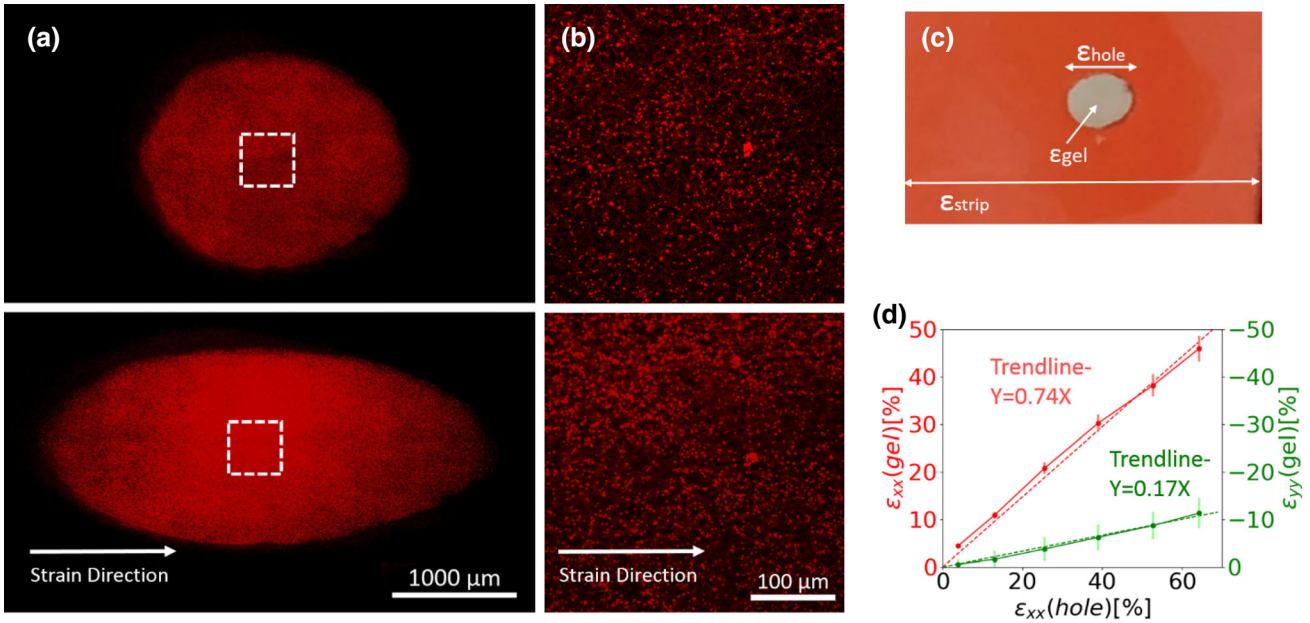

FIGURE 5. Gel strains due to external stretching of the silicone strip. (a) *X–Y* cross-section of an unstretched gel (top), and after application of ε_{hole} = 64% strain (bottom). (b) Zoom-in images of the dashed square area marked in (a). (c) Illustration of the three strain types considered in this study: ε_{strip} is the average strain of the entire silicone strip, ε_{hole} is the axial strain of the hole at its maximum diameter, and ε_{gel} is the axial strain in the center of the gel (as measured by the beads locations). (d) A linear relationship is measured between ε_{hole} and ε_{gel} in both *xx* direction (red line) and *yy* direction (green line).

resolution z-stack imaging of a fluorescently-labeled fibrin gel. A lower resolution z-stack tile image of the entire gel was also taken to estimate the ε_{hole} and its macro shape. The high-resolution confocal z-stack of the gel X–Y center showed an increase in fiber orientation in the direction of the external stretch as the magnitude of strain was increased (Figs. 6a–6c). Histograms of fiber angle distribution relative to the horizontal direction, indicated clear growing peaks around zero, the direction of the external strain (Fig. 6d). Specifically, an increase in the gel's NOP $\left(\text{NOP} = 2\left\langle(\cos\theta)^2\right\rangle - 1\right)$ (see "Methods") was calculated as the strain was increased (Figs. 6e and 6f). Comparison of the NOP between different z layers showed no significant variation, suggesting that the strain was relatively homogeneous throughout the z dimension (Fig. 6e, and error bars in Fig. 6f). The gel contracted along the z axis as a consequence of the Poisson effect, as quantitatively indicated by shorter lines at high strains (Fig. 6e). The reorientation of gel fibers as a function of the hole strain ε_{hole}, was found to be approximately linear under small strains and started to level off under high strains above approximately 40% (Fig. 6f).

Droplet-on-Silicone Experiments

We next compared our stretching system with the previously reported substrate-based approach used to stretch 3D gels.[13,42,52] The substrate-based approach served here as a model for a z-asymmetrical strain regime. For this type of experiment, we analyzed a gel "droplet" adhered to the surface of a full, unpunctured silicone strip (Fig. 7a). The strip was subjected to static stretching of increasing magnitudes, resulting in gel droplet strain. The strip was mounted in the inverted confocal microscope such that the droplet's tip pointed downwards, and the droplet base adhered to the silicone strip in an upper z depth (SI, Section 8). For each tested stretch magnitude, a low-resolution z-stack of the entire droplet was taken to measure the droplet's overall shape and contour (Fig. 7b), and a high-resolution z-stack of the droplet's center was acquired (tip to base) to measure fiber reorientation.

The low-resolution z-stack tile image of the droplet shape enabled measurement of droplet perimeters and edge-to-edge strain at different z heights (Fig. 7c). The perimeter analysis showed that the strain decreased approximately linearly as the z depth increased (Fig. 7d). Within the first 50 μm away from the silicone strip, the strain diminished by approximately 0.7–0.2% per micron, making the gel approximately 11–37% less strained after 50 μm, compared to the slice adjacent to the silicone strip. This trend continued up to the middle of the droplet, where the measurement errors of this method became too large (Fig. 7d).

In addition to the perimeter analysis, fiber orientation analysis was used to assess the z-dependent effect. Similar to the method used with the punctuated sili-

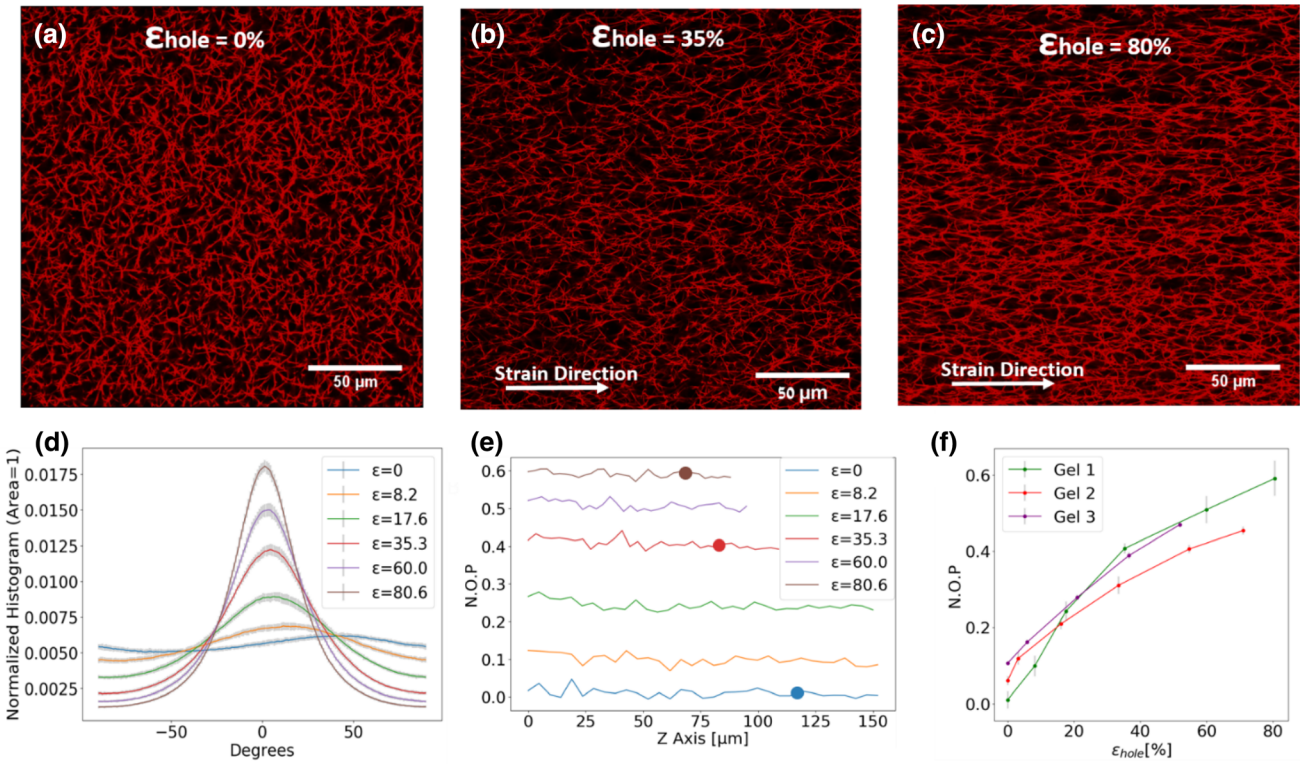

FIGURE 6. Gel fiber alignment in response to external stretch. Images taken at the center of the gel (fluorescently-labeled gel) of (a) unstretched, (b) after application of ε_{hole} = 35% and (c) ε_{hole} = 80%. (d) Averaged histograms of fiber orientations under increasing ε_{hole} strains. Grey error bars indicate differences between 40 slices in the *z*-stack assessed for each tested strain. (e) The Nematic Order Parameter (NOP) as a function of *z* height in the gel for different strain magnitudes, with *X* = 0 being the bottom of the gel. The blue dot corresponds to NOP calculated from the image in Fig. 5a, the red dot corresponds to the image in Fig. 5b, and the brown dot corresponds to the image in Fig. 5c. (f) Averaged NOP as a function of ε_{hole} for three gel repetitions (including "Gel 1" that is analyzed in (a–e).

cone strip, analysis of NOP at the central area of the gel showed an overall increase in alignment of fibers as the gel became more strained (Fig. 7e). However, as the magnitude of the external strain increased, a layer-dependent effect developed, in which slices closer to the silicone strip exhibited a higher NOP than slices near the tip (Fig. 7e). This indicates that fibers closer to the silicone are more susceptible to reorientation than fibers near the tip. Of note, imaging at depths > 200 μm was associated with reduced optical quality and errors, generally resulting in a lower calculated NOP. However, even though the calculated NOP of the base layer was optically poorer, the NOP was still greater than the NOP of the tip layers. Namely, with improved optics, the *z*-dependent effect on reorientation will be even greater than shown in this work.

Cellular Experiment

As a proof of concept that the device can provide suitable environment for cell culture, we embedded fibroblast cells in the fibrin gel, and exposed the cells to 7% static axial strain (ε_{hole}) for 5 h, in the confocal microscope (Fig. 8). *Z*-stack confocal images of cells indicate that they kept their spread morphology with long protrusions after 3 and 5 h post-stretching (Figs. 8b and 8c). The manner cells respond to the strain field should be investigated in more detail in future experiments.

DISCUSSION

This work introduces an approach and device specifically designed to strain 3D soft samples under the confocal microscopy. We demonstrated that standard commercial silicone sheets can be used as mounts for gel samples, instead of tailor-made PDMS chambers or other sheets.[12,43] The stretching system enabled *in situ* stretching of extremely soft gels (less than 1 KPa), using volumes of only a few microliters, while straining the gels in a uniform 3D fashion from its perimeter. The device was specifically designed from

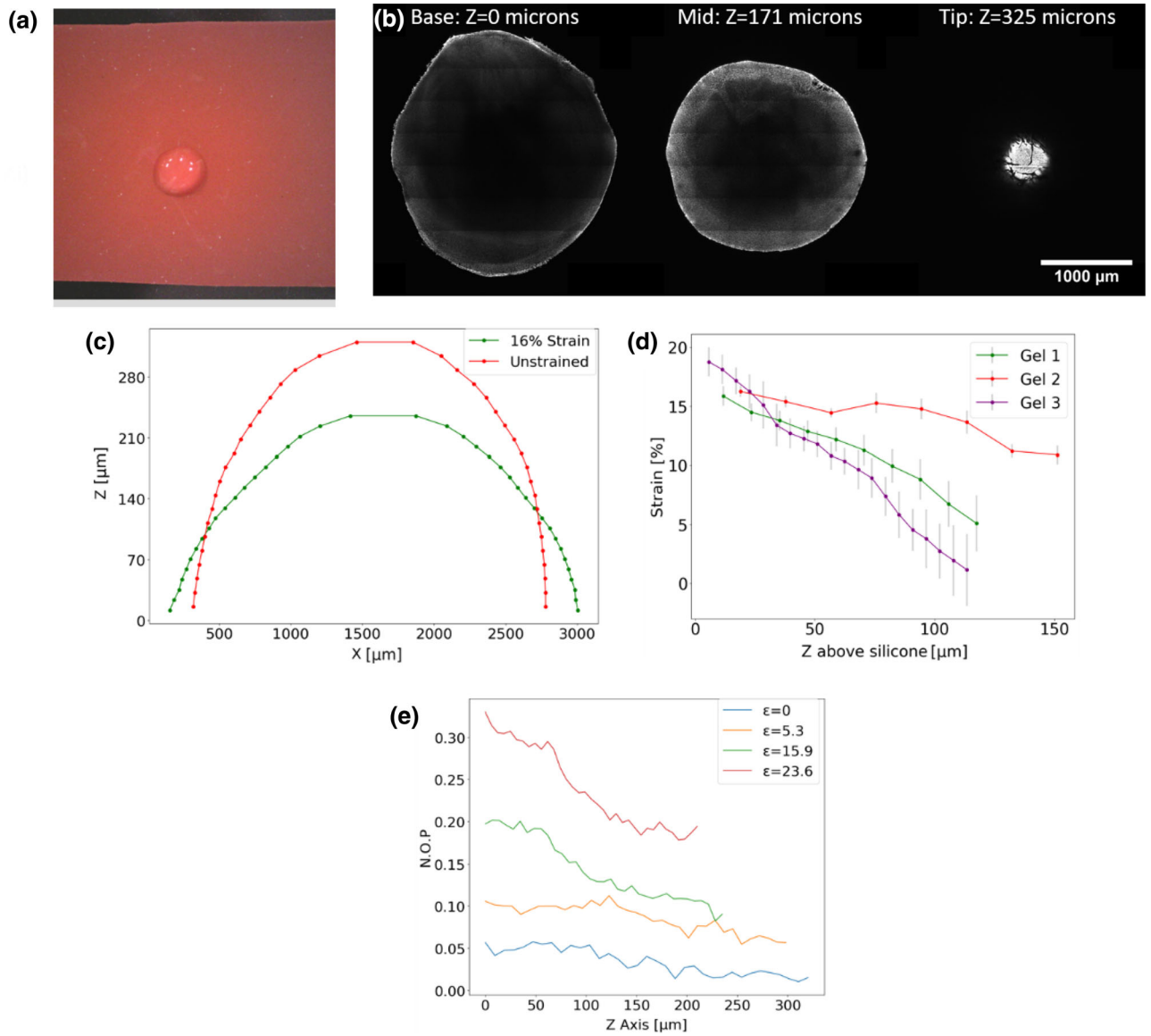

FIGURE 7. Droplet-on-silicone experiments. (a) A gel droplet adhered on top of the silicone strip. (b) Droplet of an unstretched gel imaged at three different *z* heights from the silicone strip. Since the droplet is attached upside down, canonical *z* decreased as the imaging approached the tip. (c) Gel droplet *X–Z* profile as extracted from perimeter analysis before and after subjection to 16% strain. (d) Strain as a function of distance from the silicone strip for three different droplet replicates, measured by perimeter analysis. The graph ends at about the middle of the height of the droplet, when the measurement errors began to make the data unreliable. (e) NOP calculated from the fiber orientation histograms for a single droplet, with zero being the base slice adjacent to the silicone strip. The strain values shown in the legend were calculated according to the base slice perimeter change. In all three graphs c–e, the green curve corresponds to the same gel.

3D printing parts, allowing easy replication and upgrade of the set-up in other labs.

Computer simulations of the gel-silicone setup indicates that the gel axially stretched and perpendicular compressed, due to the Poisson effect. Given a circular-shaped puncture, most of the gel area strained relatively uniformly in the X–Y plane, with strain peaking slightly near the upper and lower edge of the gel (Y-axis, Figs. 4b and 4c). Therefore, in the experiments, we analyzed the central area of the gel and data was not collected for other X–Y areas. In the experiments, the data collected with the punctured silicone strip set-up demonstrated that a 200 μm-thick 3D fibrin gel can be stretched up to 80% strain (axial strain of the punctuate central axis, ε_{hole}) while demonstrating relatively uniform response between different layers in the depth of the gel (z direction). Knowing the relationship between ε_{hole} and ε_{gel} (gel strain at the center of the gel) can provide a simple way of predicting the internal gel strains based on mea-

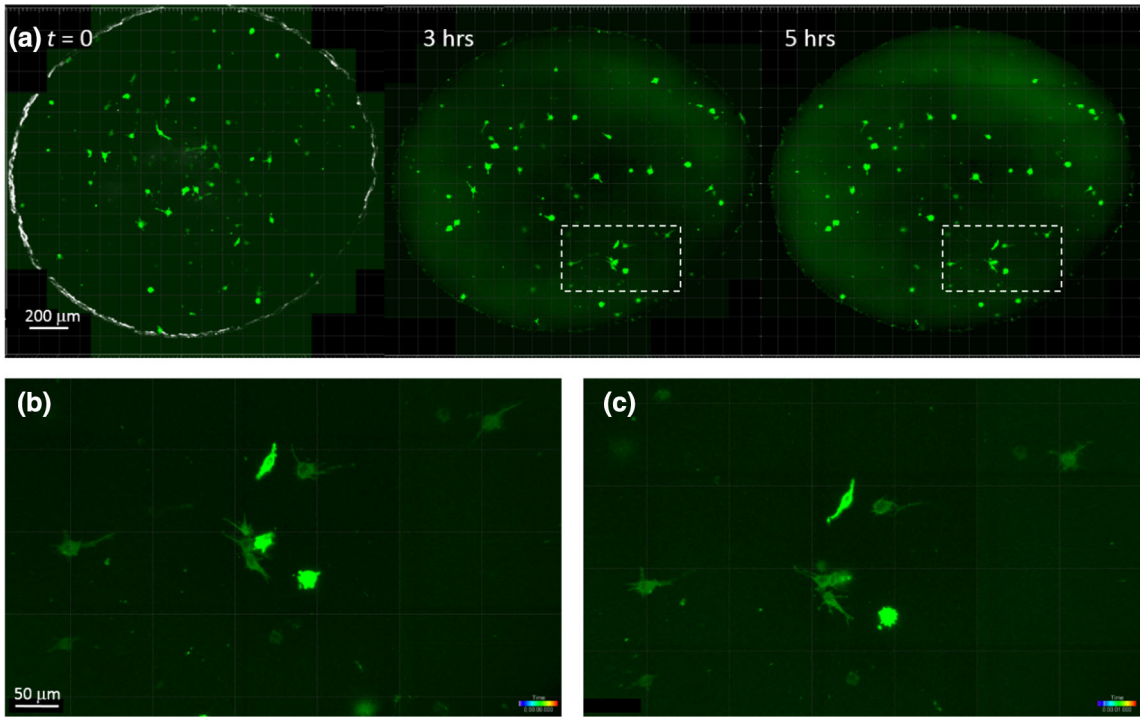

FIGURE 8. Cells grown and strained in gels on the SCyUS system. (a) Fibroblast cells (labeled with actin-GFP, green) were embedded in a fibrin gel, placed in the SCyUS system (t = 0) and strained to 7% ε_{hole} for 5 h. Maximum intensity projection images of the entire 3D circular gel at 0, 3 and 5 h post stretch. (b, c) High-resolution images of cells from the marked areas in (a). Cells were observed to spread and extended protrusions, indicating they were alive and functioning during the experiment.

surement of the external strain of the silicone hole. We found a linear relation between ε_{hole} and ε_{gel} with a slope of approximately 0.74, while in the ideal case of the simulations, a linear slope of 1 was measured. This might be the result of the discrete fibrous nature of the gel, which was not considered in the simulations. The experimentally derived slope is also likely sensitive to other parameters, such as local variations in the gel density and stiffness and z-axis geometry of the gel. Thus, if the exact magnitude of ε_{gel} is needed, the "transfer factor" ε_{hole} to ε_{gel} should be measured per experiment, and per gel location.

Gel straining clearly induced fiber alignment along the direction of the external stretch. The NOP (alignment measure) was found to increase in a nonlinear manner with strain (ε_{hole}), while the slope of the NOP-ε_{hole} curve gradually decrease. The nonlinearity of the NOP-ε_{hole} curve could be a consequence of several mechanisms. First, most of the gel fibers may have reached a very high oriented state (NOP of 0.5–0.6) after which an additional increase in strain contributes mainly to the elongation of already oriented fibers, without further contributing to an increase in the NOP. Second, based on the theoretical formulation described in Ref. 17, the nonlinearity of the NOP-Strain curve depends on the Poisson ratio. In our case, the Poisson ratio of an elastic puncture and of a gel inside said puncture is not constant, but decreases as the strain increases. This can explain the overall decrease in the slope of the curve as the strain was elevated. Finally, at high strains, optical restrictions and increased fiber density give rise to errors in fiber orientation calculations. Previous experimental works that measured the relationship between external strain and fiber alignment, are relatively limited but have demonstrated a similar decrease in slope after a significant strain was achieved.[3,35,45]

Droplet-on-silicone experiments, in which a gel droplet is adhered on top of a silicone strip, provide a unique perspective on the advantages of the punctured silicone strip and the SCyUS concept. When the gel was stretched from its underlying silicone substrate, the axial strains and fiber alignment rapidly decreased as a function of the z-depth. This effect contrasted the uniform z-deformations achieved when the gel was stretched from its circumference using the punctuated silicone approach. It therefore highlights some of the challenges of stretching soft 3D constructs from the underline substrate and other mechanism that are asymmetrical in z due to potential non-homogeneous deformations.[26,29] We note that the specific decay profile of x-strains in the z direction will depend on the macroscopic shape of the gel. In our case, we used a droplet shape as it was technically feasible, even

though it adds complexity due to the asymmetry in the z-axis. In general, we expect to witness a decay in the x-strain along the z-axis in all cases of hydrogels stretched using the substrate-based approach, whereas in the case of the punctured silicone with perimeter straining, there is no detectable decay along the z-axis.

The presented data strongly highlight an important issue that must be considered when using substrate-based or other asymmetrical approaches to stretch soft thick constructs. In general, most works presenting gel stretcher devices focus on characterizing the stress and strain profiles in the X–Y plane, which is reasonable when straining cellular monolayers. However, when using thick samples, the effect of the straining mechanism in all three dimensions of the construct should be considered and characterized. In addition, we believe that more basic study of how the ECM align and deform in 3D under external strain is of paramount importance due to the seeming lack of consensus in the field of 3D cell-seeded construct straining. Some studies have found cells to align perpendicular to the strain direction, some have found them to align parallel to strain direction and others failed to determine any directionality, with boundary conditions and stretching protocol influencing the results.[2,4,6,9,14,24,37] It is not always clear if cells align and migrate along the ECM alignment, or due to other mechanisms which came into play.[22] Though few works have decoupled the response of the ECM and cells in short term cyclic straining experiments,[53] a limited data exists on how the non-cellular ECM deforms under strain in 3D, and how this deformation may affect cell activity. Therefore, a more accurate understanding of how the ECM deforms and aligns in response to external strain, particularly in the case of 3D thick constructs, is needed.

For future application, we note that hole geometry can play a vital role in the internal strains that would develop in the gel. Previous works have shown that different sample geometries can induce different x–y strain gradients, which may be useful for basic research or specific tissue engineering applications[48] and could be an avenue for future system development. For example, stretching a diamond-shaped gel could potentially lead to a gradient in the strain regimes due to a gradual change in the initial length of the hole (along the direction of the stretch). This method of gel strain control is especially appealing in this set-up, as different shaped holes are relatively trivial to manufacture. All 2D shapes are possible, although they should conform to some basic criteria (see SI, Section 9).

Although the presented system is capable of supporting many experimental use cases, the design can be considerably improved. For example, X translation can be mostly reduced by stretching the strip from both directions, using two motors or by looping the anchored strip back to the turning spindle. Moreover, strength and probability of full gel adhesion to the strip puncture can be improved by modifications or chemical treatment of the puncture circumference, and protocols and add-ons for sterilization operation can be designed. As the CAD and code are made available here under Creative Commons (Attribution-NonCommercial-ShareAlike 4.0 International) license, we encourage other research groups to improve the design and publish their upgrades.

ELECTRONIC SUPPLEMENTARY MATERIAL

The online version of this article (https://doi.org/10.1007/s10439-019-02426-7) contains supplementary material, which is available to authorized users.

REFERENCES

[1]Bleuel, J., F. Zaucke, G. P. Bruggemann, and A. Niehoff. Effects of cyclic tensile strain on chondrocyte metabolism: a systematic review. *PLoS ONE* 10:e0119816, 2015.
[2]Bono, N., D. Pezzoli, L. Levesque, C. Loy, G. Candiani, G. B. Fiore, and D. Mantovani. Unraveling the role of mechanical stimulation on smooth muscle cells: a comparative study between 2D and 3D models. *Biotechnol. Bioeng.* 113:2254–2263, 2016.
[3]Brown, A. E. X., R. I. Litvinov, D. E. Discher, P. K. Purohit, and J. W. Weisel. Multiscale mechanics of fibrin polymer: gel stretching with protein unfolding and loss of water. *Science* 325:741–744, 2009.
[4]Carroll, S. F., C. T. Buckley, and D. J. Kelly. Cyclic tensile strain can play a role in directing both intramembranous and endochondral ossification of mesenchymal stem cells. *Front. Bioeng. Biotechnol.* 5:73, 2017.
[5]CellScale. MCT6 Stretcher.
[6]Chen, K., A. Vigliotti, M. Bacca, R. M. McMeeking, V. S. Deshpande, and J. W. Holmes. Role of boundary conditions in determining cell alignment in response to stretch. *Proc. Natl. Acad. Sci. USA* 115:986–991, 2018.
[7]Cui, Y. D., F. M. Hameed, B. Yang, K. Lee, C. Q. Pan, S. Park, and M. Sheetz. Cyclic stretching of soft substrates induces spreading and growth. *Nat. Commun.* 6:6333, 2015.
[8]de Jonge, N., J. Foolen, M. C. P. Brugmans, S. H. M. Sontjens, F. P. T. Baaijens, and C. V. C. Bouten. Degree of Scaffold degradation influences collagen (re)orientation in engineered tissues. *Tissue Eng. Part A* 20:1747–1757, 2014.
[9]de Jonge, N., F. M. W. Kanters, F. P. T. Baaijens, and C. V. C. Bouten. Strain-induced collagen organization at the micro-level in fibrin-based engineered tissue constructs. *Ann. Biomed. Eng.* 41:763–774, 2013.
[10]De, R., A. Zemel, and S. A. Safran. Dynamics of cell orientation. *Nat. Phys.* 3:655–659, 2007.
[11]EPFL Switzerland. OrientationJ plug in. 2019.
[12]Flexcell. Linear Tissue Train® Culture Plate. 2019.
[13]Flexcell. Tissue Train®. 2019.

[14]Foolen, J., V. S. Deshpande, F. M. W. Kanters, and F. P. T. Baaijens. The influence of matrix integrity on stress-fiber remodeling in 3D. *Biomaterials* 33:7508–7518, 2012.
[15]Gomez, D., S. Natan, Y. Shokef, and A. Lesman. Mechanical interaction between cells facilitates molecular transport. *Adv. Biosystems*, 2019. https://doi.org/10.1002/adbi.201900192.
[16]Gonzalez-Avalos, P., M. Murnseer, J. Deeg, A. Bachmann, J. Spatz, S. Dooley, R. Eils, and E. Gladilin. Quantification of substrate and cellular strains in stretchable 3D cell cultures: an experimental and computational framework. *J. Microsc.* 266:115–125, 2017.
[17]Goren, S., Y. Koren, X. Xu, A. Lesman A. Elastic anisotropy governs the decay of cell-induced displacements. http://arxiv.org/abs/1905.04345, 2019.
[18]Heher, P., B. Maleiner, J. Pruller, A. H. Teuschl, J. Kollmitzer, X. Monforte, S. Wolbank, H. Redl, D. Runzler, and C. Fuchs. A novel bioreactor for the generation of highly aligned 3D skeletal muscle-like constructs through orientation of fibrin via application of static strain. *Acta Biomater.* 24:251–265, 2015.
[19]Huang, G. Y., F. Li, X. Zhao, Y. F. Ma, Y. H. Li, M. Lin, G. R. Jin, T. J. Lu, G. M. Genin, and F. Xu. Functional and biomimetic materials for engineering of the three-dimensional cell microenvironment. *Chem. Rev.* 117:12764–12850, 2017.
[20]Humphrey, J. D., P. B. Wells, S. Baek, J. J. Hu, K. McLeroy, and A. T. Yeh. A theoretically-motivated biaxial tissue culture system with intravital microscopy. *Biomech. Model. Mechanobiol.* 7:323–334, 2008.
[21]Kamble, H., M. J. Barton, M. Jun, S. Park, and N. T. Nguyen. Cell stretching devices as research tools: engineering and biological considerations. *Lab Chip* 16:3193–3203, 2016.
[22]Landau, S., A. Moriel, A. Livne, M. H. Zheng, E. Bouchbinder, and S. Levenberg. Tissue-level mechanosensitivity: predicting and controlling the orientation of 3D vascular networks. *Nano Lett.* 18:7698–7708, 2018.
[23]Li, Y. H., G. Y. Huang, B. Gao, M. X. Li, G. M. Genin, T. J. Lu, and F. Xu. Magnetically actuated cell-laden microscale hydrogels for probing strain-induced cell responses in three dimensions. *Npg Asia Mater.* 8:e238, 2016.
[24]Li, Y. H., G. Y. Huang, M. X. Li, L. Wang, E. L. Elson, T. J. Lu, G. M. Genin, and F. Xu. An approach to quantifying 3D responses of cells to extreme strain. *Sci. Rep.* 6:19550, 2016.
[25]Li, Y. H., G. Y. Huang, X. H. Zhang, L. Wang, Y. A. Du, T. J. Lu, and F. Xu. Engineering cell alignment in vitro. *Biotechnol. Adv.* 32:347–365, 2014.
[26]Liu, H. J., J. Usprech, Y. Sun, and C. A. Simmons. A microfabricated platform with hydrogel arrays for 3D mechanical stimulation of cells. *Acta Biomater.* 34:113–124, 2016.
[27]Livne, A., E. Bouchbinder, and B. Geiger. Cell reorientation under cyclic stretching. *Nat. Commun.* 5:3938, 2014.
[28]Marsano, A., C. Conficconi, M. Lemme, P. Occhetta, E. Gaudiello, E. Votta, G. Cerino, A. Redaelli, and M. Rasponi. Beating heart on a chip: a novel microfluidic platform to generate functional 3D cardiac microtissues. *Lab Chip* 16:599–610, 2016.
[29]Moraes, C., M. Likhitpanichkul, C. J. Lam, B. M. Beca, Y. Sun, and C. A. Simmons. Microdevice array-based identification of distinct mechanobiological response profiles in layer-specific valve interstitial cells. *Integr. Biol.* 5:673–680, 2013.
[30]Munster, S., L. M. Jawerth, B. A. Leslie, J. I. Weitz, B. Fabry, and D. A. Weitz. Strain history dependence of the nonlinear stress response of fibrin and collagen networks. *Proc. Natl. Acad. Sci. USA* 110:12197–12202, 2013.
[31]Niklason, L. E., A. T. Yeh, E. A. Calle, Y. Bai, A. Valentin, and J. D. Humphrey. Enabling tools for engineering collagenous tissues integrating bioreactors, intravital imaging, and biomechanical modeling. *Proc. Natl. Acad. Sci. USA* 107:3335–3339, 2010.
[32]Pampaloni, F., E. G. Reynaud, and E. H. K. Stelzer. The third dimension bridges the gap between cell culture and live tissue. *Nat. Rev. Mol. Cell Biol.* 8:839–845, 2007.
[33]Panzetta, V., S. Fusco, and P. A. Netti. Cell mechanosensing is regulated by substrate strain energy rather than stiffness. *Proc. Natl. Acad. Sci. USA* 116:22004–22013, 2019.
[34]Pennisi, C. P., C. G. Olesen, M. de Zee, J. Rasmussen, and V. Zachar. Uniaxial cyclic strain drives assembly and differentiation of skeletal myocytes. *Tissue Eng. Part A* 17:2543–2550, 2011.
[35]Riching, K. M., B. L. Cox, M. R. Salick, C. Pehlke, A. S. Riching, S. M. Ponik, B. R. Bass, W. C. Crone, Y. Jiang, A. M. Weaver, K. W. Eliceiri, and P. J. Keely. 3D collagen alignment limits protrusions to enhance breast cancer cell persistence. *Biophys. J.* 107:2546–2558, 2014.
[36]Riehl, B. D., J. H. Park, I. K. Kwon, and J. Y. Lim. Mechanical stretching for tissue engineering: two-dimensional and three-dimensional constructs. *Tissue Eng. Part B* 18:288–300, 2012.
[37]Rubbens, M. P., A. Driessen-Mol, R. A. Boerboom, M. M. J. Koppert, H. C. van Assen, B. M. T. Romeny, F. P. T. Baaijens, and C. V. C. Bouten. Quantification of the temporal evolution of collagen orientation in mechanically conditioned engineered cardiovascular tissues. *Ann. Biomed. Eng.* 37:1263–1272, 2009.
[38]Schindelin, J., I. Arganda-Carreras, E. Frise, V. Kaynig, M. Longair, T. Pietzsch, S. Preibisch, C. Rueden, S. Saalfeld, B. Schmid, J. Y. Tinevez, D. J. White, V. Hartenstein, K. Eliceiri, P. Tomancak, and A. Cardona. Fiji: an open-source platform for biological-image analysis. *Nat. Methods* 9:676–682, 2012.
[39]Schurmann, S., S. Wagner, S. Herlitze, C. Fischer, S. Gumbrecht, A. Wirth-Hucking, G. Prolss, L. A. Lautscham, B. Fabry, W. H. Goldmann, V. Nikolova-Krstevski, B. Martinac, and O. Friedrich. The IsoStretcher: an isotropic cell stretch device to study mechanical biosensor pathways in living cells. *Biosens. Bioelectron.* 81:363–372, 2016.
[40]Sears, C., and R. Kaunas. The many ways adherent cells respond to applied stretch. *J. Biomech.* 49:1347–1354, 2016.
[41]Storm, C., J. J. Pastore, F. C. MacKintosh, T. C. Lubensky, and P. A. Janmey. Nonlinear elasticity in biological gels. *Nature* 435:191–194, 2005.
[42]STREX. STB-150. 2019.
[43]STREX. Stretch Chambers. 2019.
[44]Tondon, A., H. J. Hsu, and R. Kaunas. Dependence of cyclic stretch-induced stress fiber reorientation on stretch waveform. *J. Biomech.* 45:728–735, 2012.
[45]Vader, D., A. Kabla, D. Weitz, and L. Mahadevan. Strain-induced alignment in collagen gels. *PLoS ONE* 4:5902, 2009.
[46]Walker, M., M. Godin, and A. E. Pelling. A vacuum-actuated microtissue stretcher for long-term exposure to oscillatory strain within a 3D matrix. *Biomed. Microdevices* 20:43, 2018.

[47]Walters, B., T. Uynuk-Ool, M. Rothdiener, J. Palm, M. L. Hart, J. P. Stegemann, and B. Rolauffs. Engineering the geometrical shape of mesenchymal stromal cells through defined cyclic stretch regimens. *Sci. Rep*. 7:6640, 2017.

[48]Wang, L., Y. H. Li, B. Chen, S. B. Liu, M. X. Li, L. Zheng, P. F. Wang, T. J. Lu, and F. Xu. Patterning cellular alignment through stretching hydrogels with programmable strain gradients. *ACS Appl. Mater. Interfaces* 7:15088–15097, 2015.

[49]Weidenhamer, N. K., and R. T. Tranquillo. Influence of cyclic mechanical stretch and tissue constraints on cellular and collagen alignment in fibroblast-derived cell sheets. *Tissue Eng. Part C* 19:386–395, 2013.

[50]Wen, Q., A. Basu, P. A. Janmey, and A. G. Yodh. Non-affine deformations in polymer hydrogels. *Soft Matter* 8:8039–8049, 2012.

[51]Wen, Q., A. Basu, J. P. Winer, A. Yodh, and P. A. Janmey. Local and global deformations in a strain-stiffening fibrin gel. *New J. Phys*. 9:428, 2007.

[52]Yung, Y. C., H. Vandenburgh, and D. J. Mooney. Cellular strain assessment tool (CSAT): precision-controlled cyclic uniaxial tensile loading. *J. Biomech*. 42:178–182, 2009.

[53]Zhao, R. G., T. Boudou, W. G. Wang, C. S. Chen, and D. H. Reich. Decoupling cell and matrix mechanics in engineered microtissues using magnetically actuated microcantilevers. *Adv. Mater*. 25:1699–1705, 2013.